*Int. J. Electrochem. Sci.*, 17 **(2022)** Article ID: 221167, doi: 10.20964/2022.11.88

International Journal of
ELECTROCHEMICAL
SCIENCE
www.electrochemsci.org

# Electrochemical Corrosion Behaviour of X80 Steel in Sandy Soil under a Natural Air-drying State

*Ruizhen Xie[1,4*], Shuke Zhang[1], Xu Zhang[1], Ruicheng Geng[1], Yating Xie[1], Boqiong Li[1,4], Pengju Han[2*], Baojie Dou[3], Zhenxia Wang[5]*

[1] Department of Materials Science and Engineering, Jinzhong University, Jinzhong 030600, China
[2] Department of Civil Engineering, Taiyuan University of Technology, Taiyuan 030024, China
[3] Material Corrosion and Protection Key Laboratory of Sichuan province, Sichuan University of Science and Engineering, Zigong 643002, China
[4] Shanxi Province Collaborative Innovation Center for Light Materials Modification and Application, Jinzhong, 030600, China
[5] College of Material Science and Engineering, Taiyuan University of Technology, Taiyuan 030024, China.
[*]E-mail: 13834569544@163.com, 18735394929@163.com

*Received:* 9 August 2022 / *Accepted:* 15 October 2022 / *Published:* 20 October 2022

Based on the relationships among electrochemical theory, corrosion of sandy soil and corrosion principle of X80 steel, the corrosion mechanism of X80 steel in sandy soil under a natural air-drying state was comprehensively studied in this paper. The results show that with increasing age, as the water content in sandy soil decreased, the polarization curve of X80 steel shifted to the upper left, and its corrosion rate gradually weakened. The X80 steel exhibited slight corrosion, and the average corrosion rate was 1.65E-2 mm/a. Near the limit volume content of the liquid bridge, the radius of the capacitive arc was the smallest, and sandy soil had the strongest corrosion effect on X80 steel. Brown-yellow corrosion products (iron oxides, $Fe_2O_3$) with uneven thickness were deposited on the surface of the X80 steel. The localized corrosion products appeared as leopard pattern, flocculent clusters, rice grains.

**Keywords:** sandy soil, X80 steel, air-drying, corrosion

## 1. INTRODUCTION

In recent years, pipeline steel is developing towards thick specification and high strength, among which X80 pipeline steel will become one of the mainstream pipeline steels. Corrosion damage to pipeline steel can cause significant economic losses and consume a large amount of resources and energy while threatening oil and gas transportation safety and personal safety. Soil corrosion is one of the main causes of buried pipeline failure, and it is highly concealed and difficult to detect. Therefore, to ensure

the safe operation of pipelines, it is necessary to comprehensively understand, analyze and judge the soil corrosion of pipelines.

Soil is a complex system composed of gas, liquid and solid three-phase substances and has the characteristics of corrosiveness, seasonality and regionality. At present, China has preliminarily established a natural environment corrosion test network [1]. The corrosion process in soil is mainly an electrochemical dissolution process, and soil and pipeline together constitute various corrosion batteries [2]. The corrosion of buried pipes in soil is a complex process involving multiscale interactions and a variety of abiotic and biotic factors, among which water content and soil quality are important influencing factors [3]. Water makes soil an electrolyte, and is a prerequisite for electrochemical corrosion. The water content in soil has a maximum value for the corrosion rate of metal materials [4].

The details of soil corrosion, as well as thermodynamic and kinetic information, can be obtained in a short period of time by electrochemical testing techniques [4, 5]. At present, the main techniques used are the linear polarization resistance technique, AC impedance technique, and Tafel slope extrapolation method. These methods are easy to operate, have a short cycle, and can obtain relatively accurate test results under the premise of reasonable testing means and steps. Electrochemical impedance spectroscopy (EIS) has been gradually extended to the fields of building materials and geotechnical engineering [6-8]. At present, the electrochemical characteristics of sand system are mainly analysed from the aspects of three-phase interface zone characteristics [9], basic model and equivalent circuit fitting [10, 11].

The electrochemical corrosion of X80 steel in a soil environment has mostly been studied in a soil simulation solution, and the main ions in simulation solution are $Cl^-$, $CO_3^{2-}$, $HCO_3^-$ and $SO_4^{2-}$ [12, 13]. There are also studies on the initial electrochemical corrosion of X80 steel in soil media such as sand [14], typical cohesive soil [15, 16], silt [17, 18] and mud [19]. X80 steel also exhibits different corrosion behaviours and corrosion laws in various soils, and corrosion has a time effect. To further explore the influence of water on the electrochemical corrosion mechanism of X80 steel in sandy soil, this paper explored the electrochemical corrosion behavior of X80 steel in sandy soil with an initial saturated water content under the condition of a continuous reduction of water content, namely, a natural air-drying state.

## 2. EXPERIMENTAL METHOD

### *2.1 Materials*

The sandy soil used in the test was Xiamen ISO standard sand with a silica content greater than 98%. The maximum dry density ($\rho_{dmax}$) was 1.86 g/cm$^3$, the minimum dry density ($\rho_{dmin}$) was 1.56 g/cm$^3$. It can be seen from the gradation curve (Figure 1) that the gradation of the standard sand is discontinuous, but it is a good grade of coarse sand, which meets the two conditions of $Cu \geq 5$ and $Cc=1\sim3$. Pure water was used as the electrolyte. The working electrode is the representative pipeline steel X80, which is characterized by low carbon content and low alloying element content, C: Si: Mn: Fe=0.063: 0.28: 1.83: 97.4. Before the test, the Φ15 ×2 mm X80 sheet was polished step by step with #360, #800 and #1500 SiC sandpaper and then ultrasonically cleaned in acetone solution for 10 min and dried. After that, a

working area of 1 $cm^2$ was left for the working electrode by wax sealing. A rubber box with an internal volume of 7.07×7.07×7.07 $cm^3$ was used as the electrolyzer. The weight of the sandy soil was 300 g, and the initial weight of water was 90 g. Weighing was performed on an electronic balance with an accuracy of 0.01.

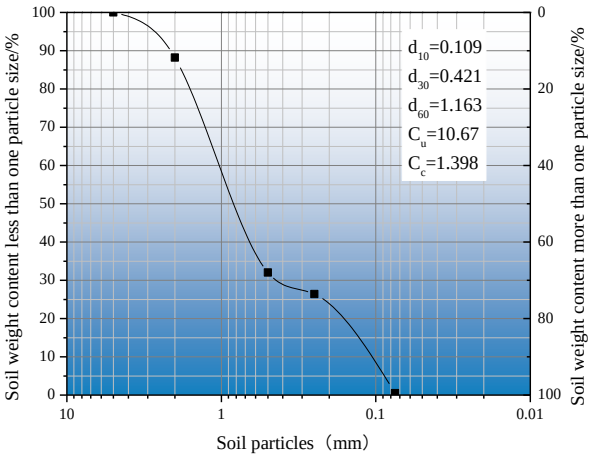


**Figure 1.** Gradation curve of the standard sand

*2.2 Method*

The initial state of the sandy soil was saturated (water content, 30%), and the test ages were 1d, 2d, 3d, …, until the sandy soil was air-dried. Under a natural air-drying state, an electrochemical test of X80 steel in sandy soil was carried out using electrochemical workstation (CS350H, Wuhan Corrtest Instruments Corp., Ltd.). The three electrodes were X80 steel (WE, working electrode), calomel electrode (RE, reference electrode) and titanium mesh (CE, counter electrode), as show in Figure 2. The test conditions of electrochemical impedance spectroscopy were an AC amplitude of 5 mV and a scanning frequency of $10^{-2}$–$10^5$ Hz. The potential range of the potentiodynamic polarization test was -1–2 V near the open circuit potential, and the scanning rate was 3 mV/s. A soil meter (FK-WSYP) was used to test the temperature, moisture and pH of the sandy soil.

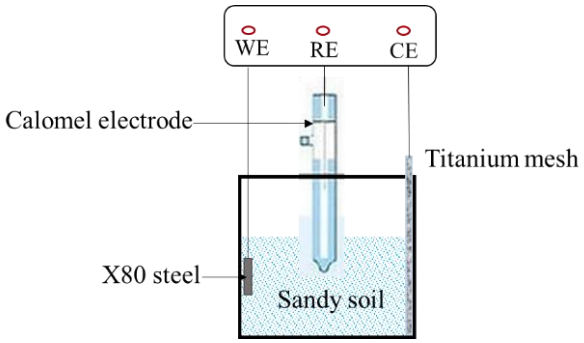


**Figure 2.** Testing device

The macroscopic corrosion morphology of the corrosion products was obtained by optical digital microscope (Olympus DSX1000), and the microscopic morphology of the corrosion products and

corroded X80 steel (×50, ×100, ×200, ×500, ×1000) were obtained by scanning electron microscope (JSM-6510, Japan Electronics Co., Ltd.). The elemental composition or chemical state of the corrosion products was analysed by energy dispersive spectroscopy (EDS) and X-ray photoelectron spectroscopy (XPS). The equipment used for EDS was an energy spectrometer (GENESIS, EDAX), and the equipment used for XPS is an X-ray photoelectron energy spectrometer (Thermo Scientific EscaLab $Xi^+$, Thermo Fisher Scientific). The sample was derusted by soaking in 50% dilute hydrochloric acid for 5-10 min.

## 3. RESULTS AND DISCUSSION

### *3.1 Physical and Chemical Properties of Sandy Soil*

The physical and chemical properties of sandy soil under the natural air-dried state are shown in Table 1. The moisture in the sand was gradually air-dried from the initial saturated state of 30% to 0% over 14 days. The pH value of the sandy soil fluctuated in a range of 6.85-7.05, and the sandy soil was basically neutral. The temperature also fluctuated around 20 °C.

**Table 1.** Physical and chemical properties of sandy soil under the natural air-dried state

| Age/d | pH | Water content /% | Temperature/℃ |
|---|---|---|---|
| 1 | 6.85 | 30.0 | 19.5 |
| 2 | 6.97 | 24.0 | 16.7 |
| 3 | 6.95 | 15.6 | 12.9 |
| 4 | 7.02 | 14.8 | 21.9 |
| 5 | 6.87 | 13.5 | 18.2 |
| 6 | 6.95 | 12.7 | 21.5 |
| 7 | 6.99 | 10.3 | 21.2 |
| 8 | 6.99 | 8.0 | 19.9 |
| 9 | 6.98 | 6.2 | 22.4 |
| 10 | 6.97 | 6.0 | 22.0 |
| 11 | 7.00 | 3.4 | 21.9 |
| 12 | 7.03 | 0.5 | 20.5 |
| 13 | 7.05 | 0.2 | 20.5 |
| 14 | 7.03 | 0.0 | 21.9 |

### *3.2 Polarization curve of X80 steel*

Figure 3 shows the polarization curve of X80 steel in sandy soil under the natural air-drying state. With increasing age, as the water content in sandy soil decreases, the polarization curve of the X80 steel shifted to the upper left as a whole, and the corrosion of the X80 steel gradually weakens. When the water content was 30%~12.7% (1-6 d), the corrosion potential of the X80 steel was approximately -1 V.

When the water content was 10.3%~0.2% (7-13 d), the corrosion potential of the X80 steel fell below -0.5 V. When the water content was 0 (14 d), the corrosion potential of X80 steel exceeded -0.5 V, and the corrosion current density was the smallest.

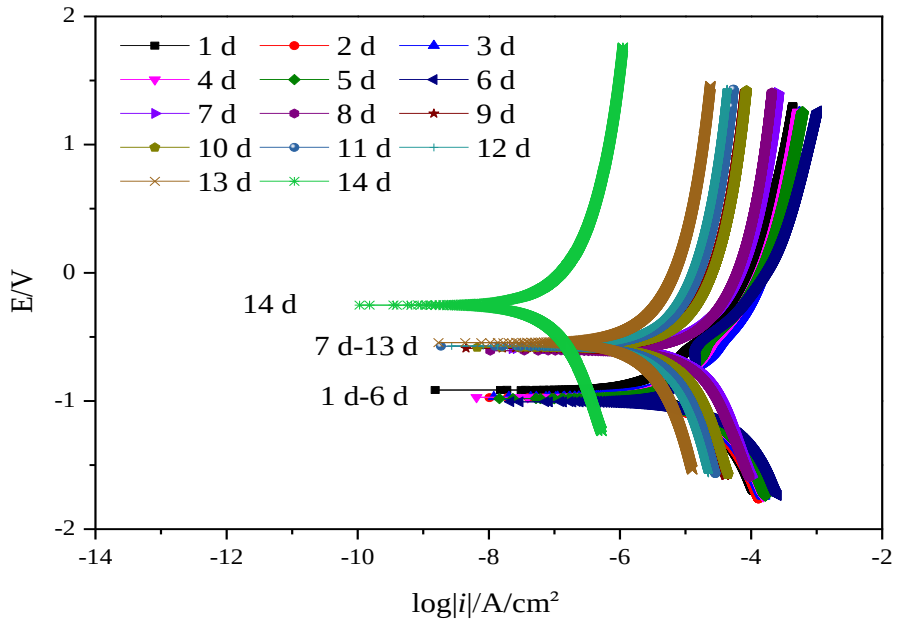


**Figure 3.** Polarization curve of X80 steel at different ages (1-14 d) in sandy soil under the natural air-dried state

**Table 2.** $R_p$ fitting results of polarization curve of X80 steel in sandy soil under the natural air-dried state

| Age/d | Corrosion Rate/mm/a | $R_p$/Ω/cm$^2$ | $I_o$/Amps/cm$^2$ | $E_o$/Volts |
|---|---|---|---|---|
| 1 | 1.11E-2 | 2.77E4 | 9.40E-7 | -0.911 |
| 2 | 1.83E-2 | 1.68E4 | 1.56E-6 | -0.972 |
| 3 | 1.98E-2 | 1.55E4 | 1.68E-6 | -0.965 |
| 4 | 2.16E-2 | 1.42E4 | 1.83E-6 | -0.968 |
| 5 | 2.36E-2 | 1.29E4 | 2.01E-6 | -0.978 |
| 6 | 3.33E-2 | 9.22E4 | 2.83E-6 | -1.002 |
| 7 | 2.98E-2 | 1.03E4 | 2.54E-6 | -0.592 |
| 8 | 2.80E-2 | 1.09E4 | 2.38E-6 | -0.608 |
| 9 | 1.27E-2 | 2.42E4 | 1.08E-6 | -0.589 |
| 10 | 1.38E-2 | 2.23E4 | 1.17E-6 | -0.582 |
| 11 | 8.69E-3 | 3.53E4 | 7.39E-7 | -0.573 |
| 12 | 6.76E-3 | 4.54E4 | 5.75E-7 | -0.570 |
| 13 | 3.77E-3 | 8.14E4 | 3.20E-7 | -0.545 |
| 14 | 1.51E-4 | 2.03E6 | 1.28E-8 | -0.253 |

To further study the corrosion rate of X80 in sandy soil, $R_p$ weak polarization fitting was carried out on the polarization curve, and the fitting interval was ±50 mV near the open circuit potential. The results are shown in Table 2. The order of magnitudes of $R_p$ (polarization resistance) was $10^4$ for the first 13 days and reached $10^6$ on the 14th day. From the $I_o$ (corrosion current density), the values were all below 3 μA/cm$^2$, and the corrosion of X80 steel in sandy soil was characterized as mild corrosion [20]. When the water content was 0% (14 d), the $E_o$ (corrosion potential) of the X80 steel reaches -0.253 V. The overall corrosion rate decreased gradually, the order of magnitude decreased from $10^{-2}$ to $10^{-4}$, and the average corrosion rate of X80 steel was 1.65E-2 mm/a.

### *3.3 Electrochemical Impedance Spectroscopy of X80 Steel*

Figure 4 shows the Nyquist diagrams of X80 steel in sandy soil under the natural air-drying state (1–14 d). With increasing age, as the water content in sandy soil decreased, the impedance spectrum fluctuates greatly in the frequency domain of $10^3$-$10^6$ Hz after 5 d. The three phases of solid, liquid and gas in the sandy soil at high frequency all constitute conductive paths, causing large fluctuations in the impedance spectrum [21]. In the frequency range of $10^{-2}$~$10^3$ Hz, the impedance spectra showed a flat capacitive reactance arc, the intersection with the real axis first shifts to the left and then to the right, and the radius of the capacitive reactance arc increased first and then decreased. At 7 d and 8 d, the water content of sandy soil was 10.3% and 8.0%, respectively, near the limit volume content of the liquid bridge (6%-12%) [21]. The corresponding capacitive arc radius reached the minimum, and the sandy soil had the strongest corrosion effect on the X80 steel.

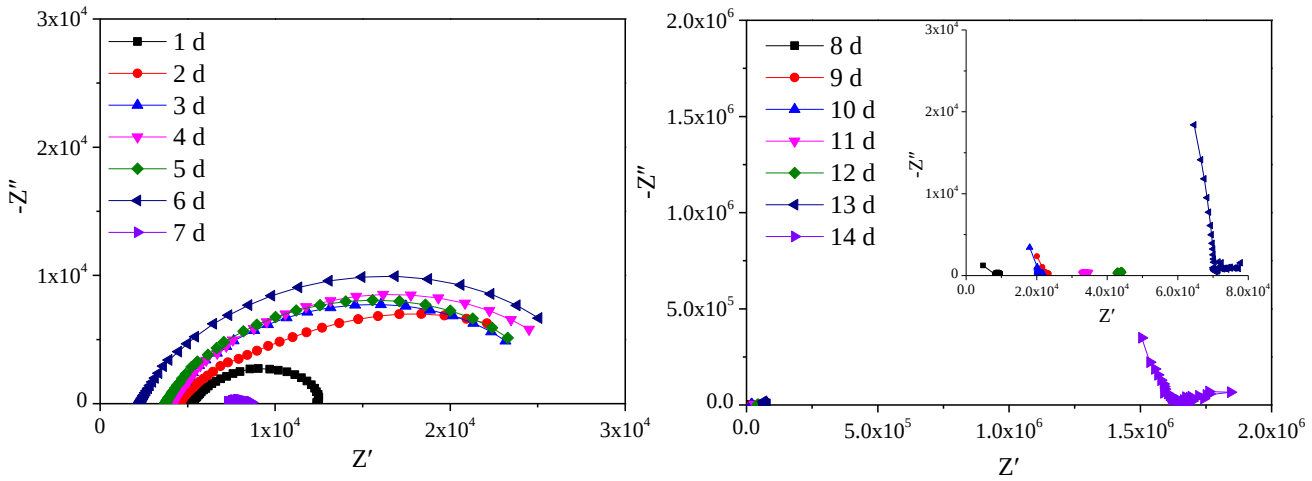


**Figure 4.** Nyquist diagrams of X80 steel at different ages (1-14 d) in sandy soil under the natural air-dried state

Figure 5 and Figure 6 show the modulus and phase angle (Theta) of the X80 steel in sandy soil under a natural air-drying state, respectively. Consistent with the law of the impedance spectrum, after 5 d, the fluctuation was larger in the frequency domain of $10^3$-$10^6$ Hz. To further study the impedance characteristics of X80 steel in sandy soil, an equivalent circuit R(C(R(Q(RW)))) (Figure 7) was selected according to the modulus and phase angle characteristics to conduct equivalent circuit fitting of the

impedance spectrum of the X80 steel. The fitting was performed on the nonfluctuating part, and the fitting results are shown in Figure 8, Figure 9 and Table 3. Figures 8 and Figures 9 show that the equivalent circuit fitting results are good.

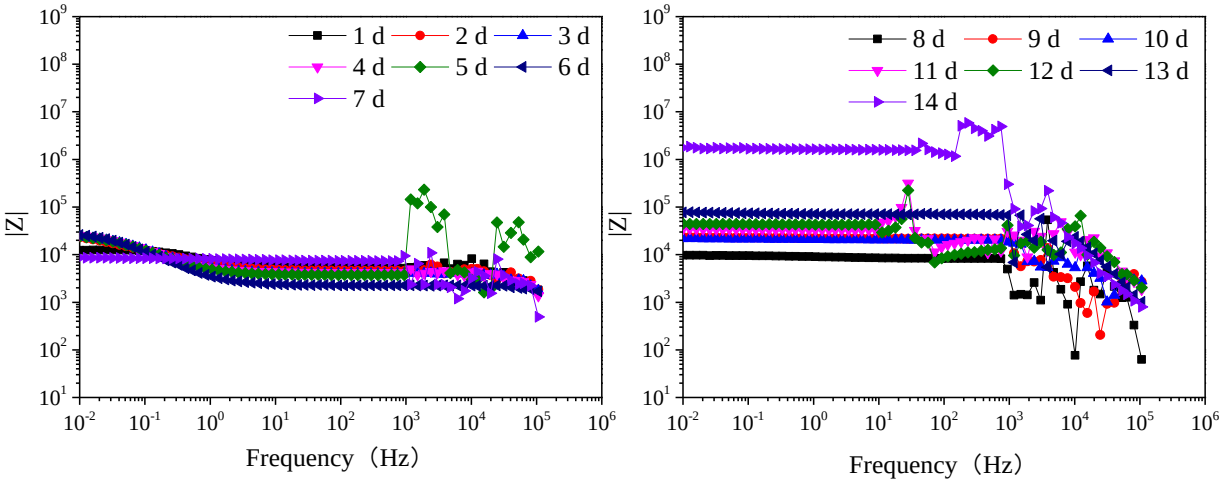


**Figure 5.** Bode diagram (modulus) of X80 steel at different ages (1-14 d) in sandy soil under the natural air-dried state

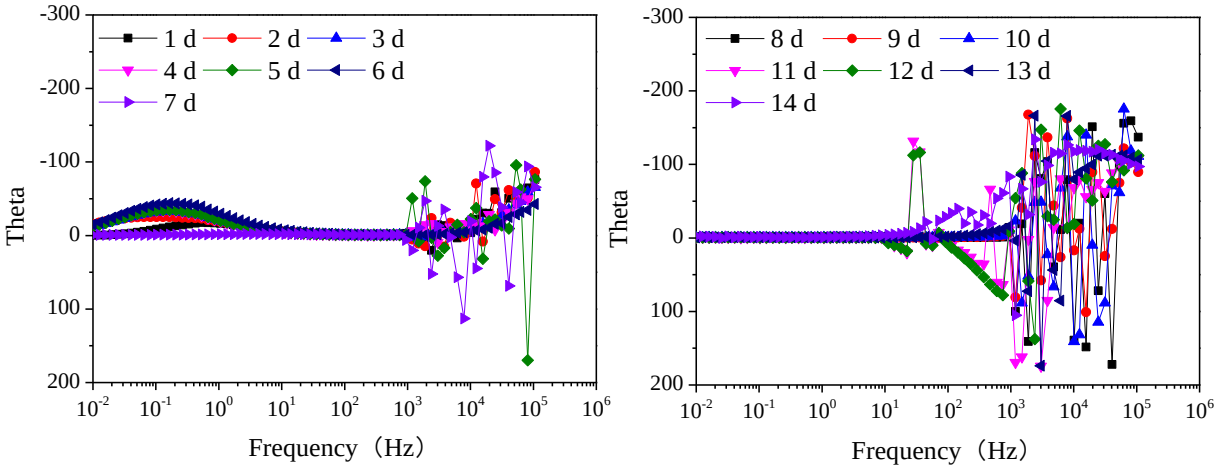


**Figure 6.** Bode diagram (Theta) of X80 steel at different ages (1-14 d) in sandy soil under the natural air-dried state

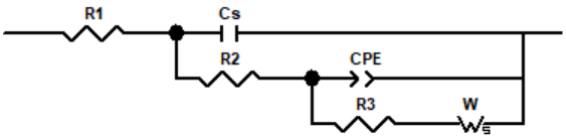


**Figure 7.** Equivalent circuit

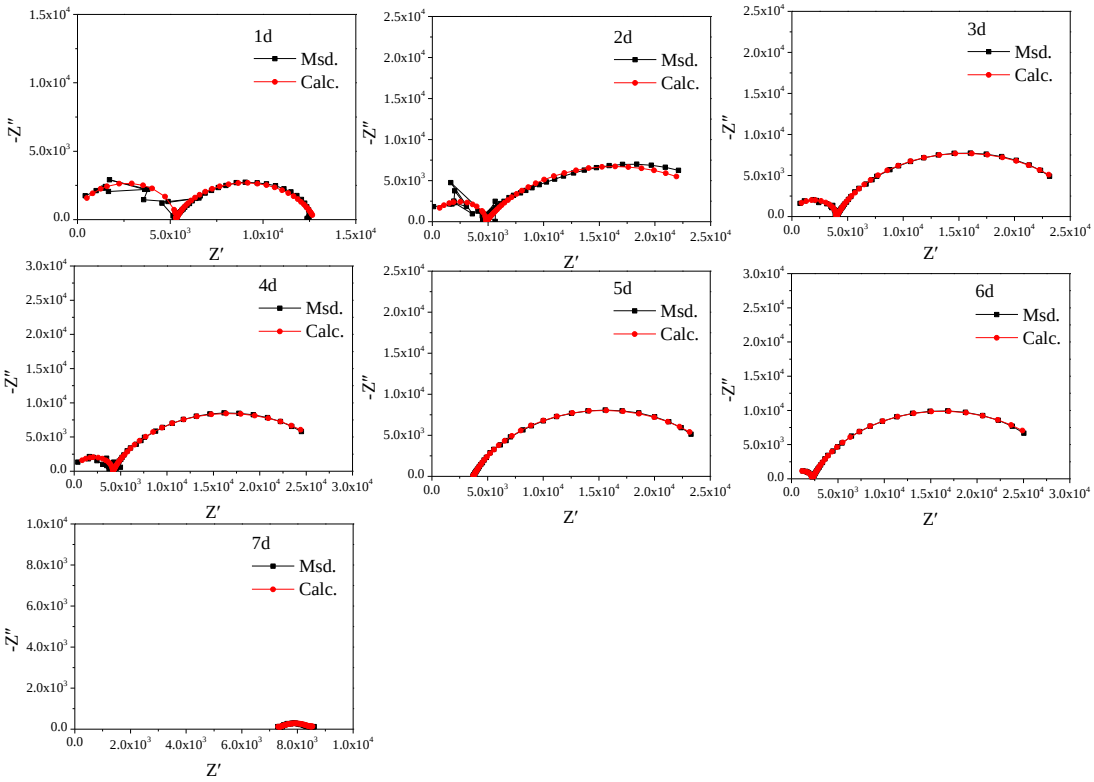


**Figure 8.** Fitting results of the impedance spectrum of X80 steel (1-7d) in sandy soil under the natural air-dried state

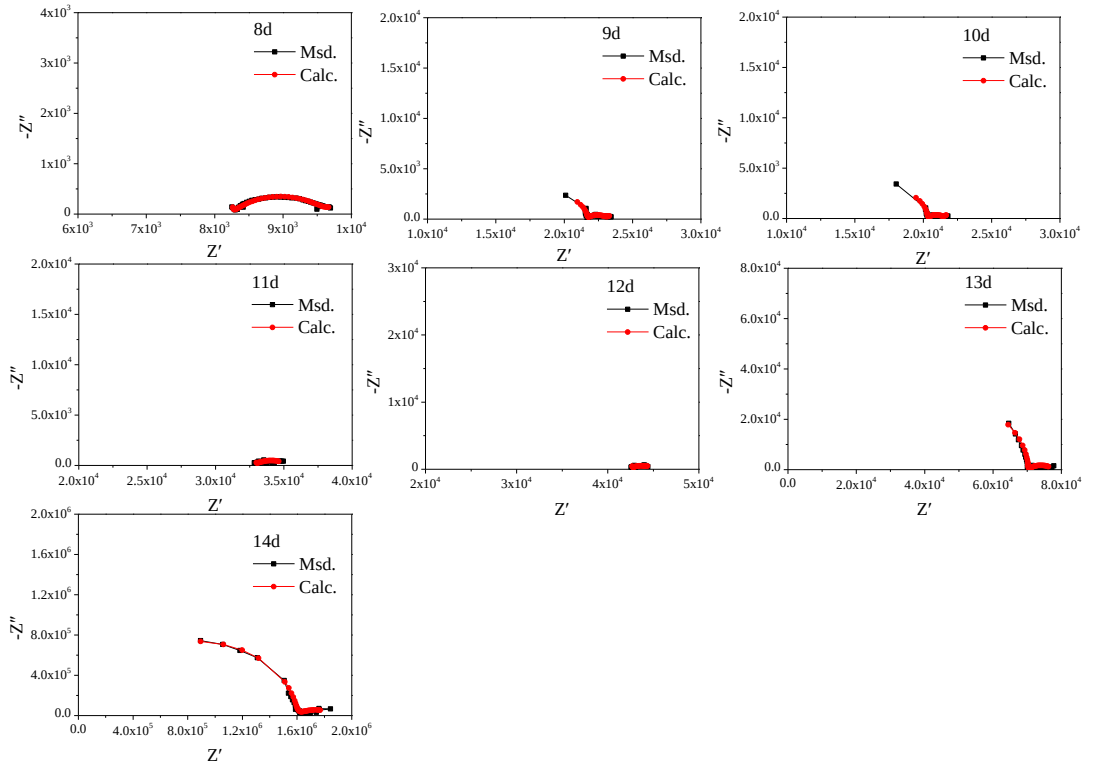


**Figure 9.** Fitting results of the impedance spectrum of X80 steel (8-14d) in sandy soil under the natural air-dried state

The results in Table 3 show that the water content reached below the limit volume of the liquid bridge (7 d and 8 d), and the fitting parameters fluctuate greatly, which may be related to the complex liquid phase distribution. With decreasing water content, the solution resistance $R_1$, sand resistance $R_2$ and charge transfer resistance $R_3$ all tended to increase, but the overall change in $R_2$ was small. In addition, W (diffusion impedance), which represents tortuosity, fluctuates greatly, which was related to the complex pore structure of sandy soil [21]. For the constant phase angle CPE, n was below 0.8, and the interface capacitance deviates from the ideal capacitance.

**Table 3.** Fitting results of impedance spectrum of X80 steel in sandy soil under the natural air-dried state

| Age/d | $R_1$ /Ω·cm$^2$ | Cs /F·cm$^{-2}$ | $R_2$ /Ω·cm$^2$ | CPE | | $R_3$/ Ω·cm$^2$ | W/ S·sˆ0.5·cm$^{-2}$ |
|---|---|---|---|---|---|---|---|
| | | | | $Y_o$/S·s$^{-n}$·cm$^{-2}$ | n | | |
| 1 | 2.47E-3 | 8.60E-10 | 5.31E3 | 5.90E-5 | 0.79 | 7.48E3 | 4.18E2 |
| 2 | 1.86E-3 | 7.70E-10 | 4.85E3 | 1.26E-4 | 0.67 | 2.31E4 | 6.13E16 |
| 3 | 4.12E-3 | 7.08E-10 | 4.01E3 | 1.12E-4 | 0.76 | 2.27E4 | 1.92E-2 |
| 4 | 1.17E2 | 7.70E-10 | 4.07E3 | 1.16E-4 | 0.76 | 2.46E4 | 1.01E-2 |
| 5 | 3.59E3 | 4.29E-7 | 1.39E2 | 1.18E-4 | 0.76 | 2.35E4 | 7.90E10 |
| 6 | 5.67E-4 | 6.50E-10 | 2.25E3 | 1.17E-4 | 0.78 | 2.79E4 | 7.17E6 |
| 7 | 7.01E3 | 2.00E-7 | 2.91E2 | 1.72E-4 | 0.54 | 1.21E3 | 2.81E-2 |
| 8 | 1.65E-1 | 3.39E-10 | 8.24E3 | 1.97E-4 | 0.58 | 1.41E3 | 3.71E-2 |
| 9 | 1.70E4 | 1.50E-8 | 4.71E3 | 1.88E-4 | 0.62 | 1.46E3 | 1.10E-2 |
| 10 | 1.44E4 | 1.17E-8 | 5.89E3 | 2.49E-4 | 0.65 | 1.18E3 | 9.99E-3 |
| 11 | 3.32E-2 | 2.18E-9 | 3.28E4 | 6.30E-4 | 0.46 | 2.56E3 | 5.86E2 |
| 12 | 1.39E-1 | 3.34E-9 | 4.26E4 | 5.29E-4 | 0.61 | 1.83E3 | 1.07E-2 |
| 13 | 9.61E3 | 9.06E-10 | 6.06E4 | 1.82E-4 | 0.54 | 7.57E3 | 9.49E5 |
| 14 | 1.04E5 | 6.88E-10 | 4.50E2 | 5.79E7 | 3.96E-3 | 1.20E7 | 1.82E-7 |

### *3.4 Electrochemical Corrosion Mechanism of X80 Steel*

Figure 10 shows the macroscopic corrosion morphology (×18) of X80 steel in sandy soil under a natural air-drying state. The results show that brown-yellow corrosion products (iron oxides) with uneven thickness were deposited on the surface of the X80 steel, which was related to the porous structure of the sandy soil. The part in contact with pore fluid can be directly electrochemically corroded, the accumulated corrosion products are more abundant, and the corresponding products were darker in color than those for other regions [22]. SEM results of corrosion products (Figure 11) show that corrosion products were shaped as leopard patterns, flocculent clusters, and rice grains, and there are cracks.

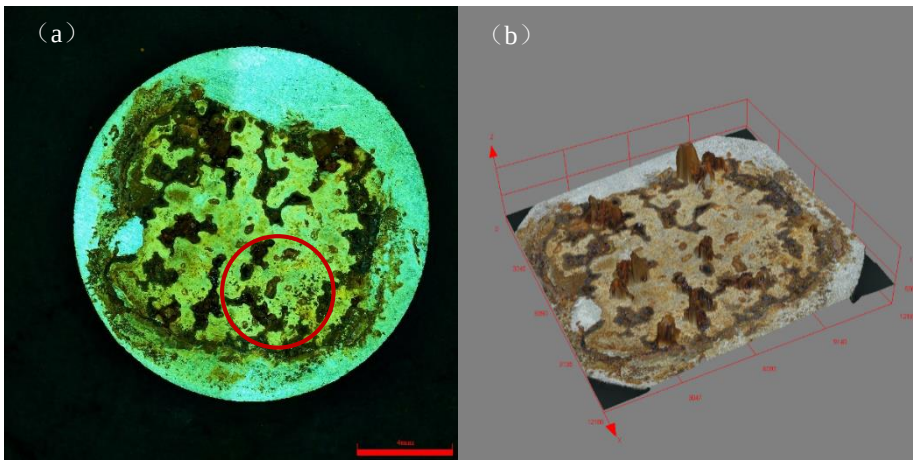


**Figure 10.** Macroscopic corrosion morphology of X80 steel: (a) 2D image (b) 3D image

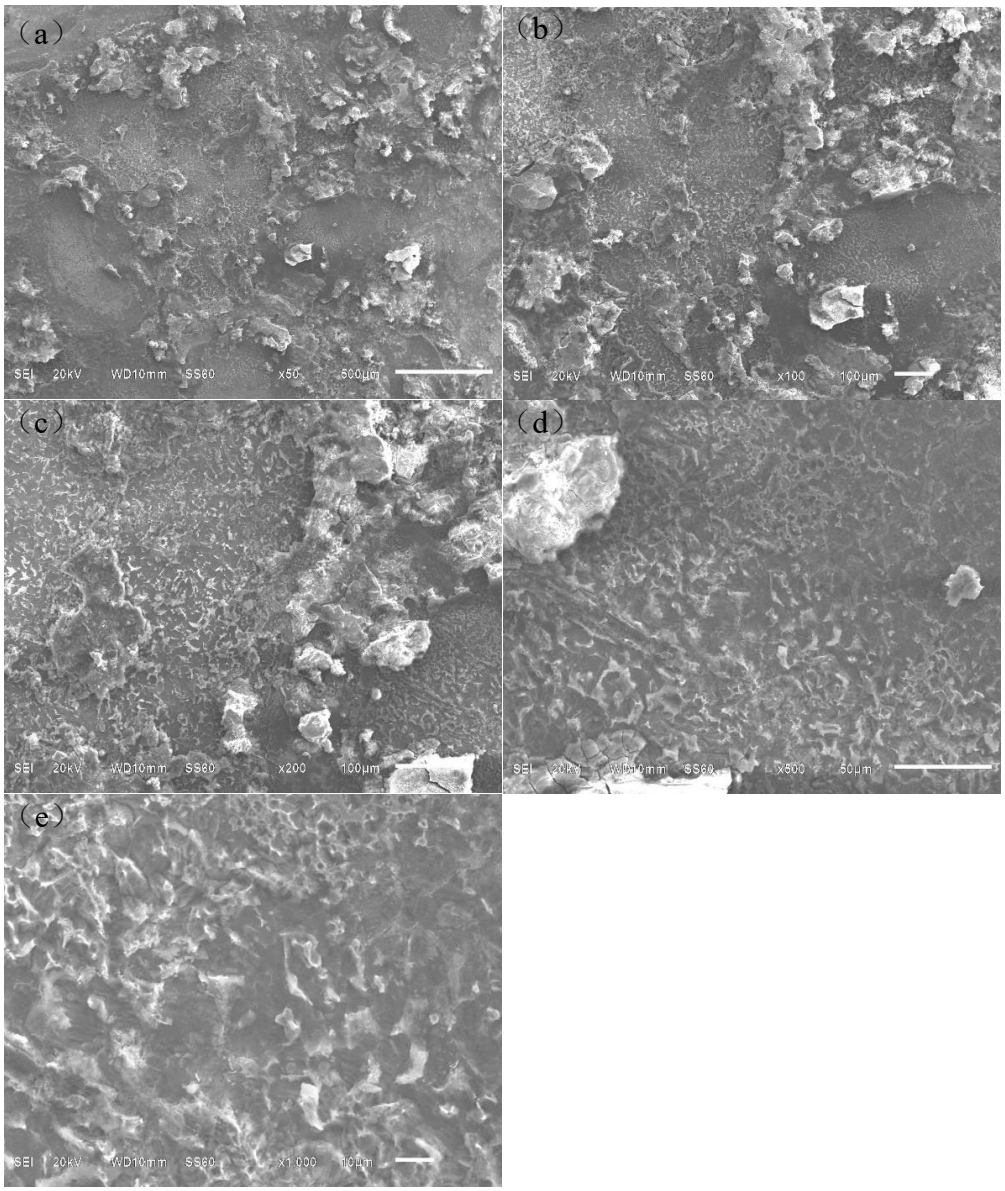


**Figure 11.** SEM of corrosion products on the surface of X80 steel: (a) × 50, (b) × 100, (c) × 200, (d) × 500, (e) × 1000

To further study the composition of corrosion products on the surface of X80 steel, EDS and XPS analyses of corrosion products selected in Figure 9 (a) were carried out in this paper. The EDS results (Figure. 12) showed that the corrosion products were mainly composed of Fe, O and C. Fe and O were the constituent elements of brown-yellow iron oxide.

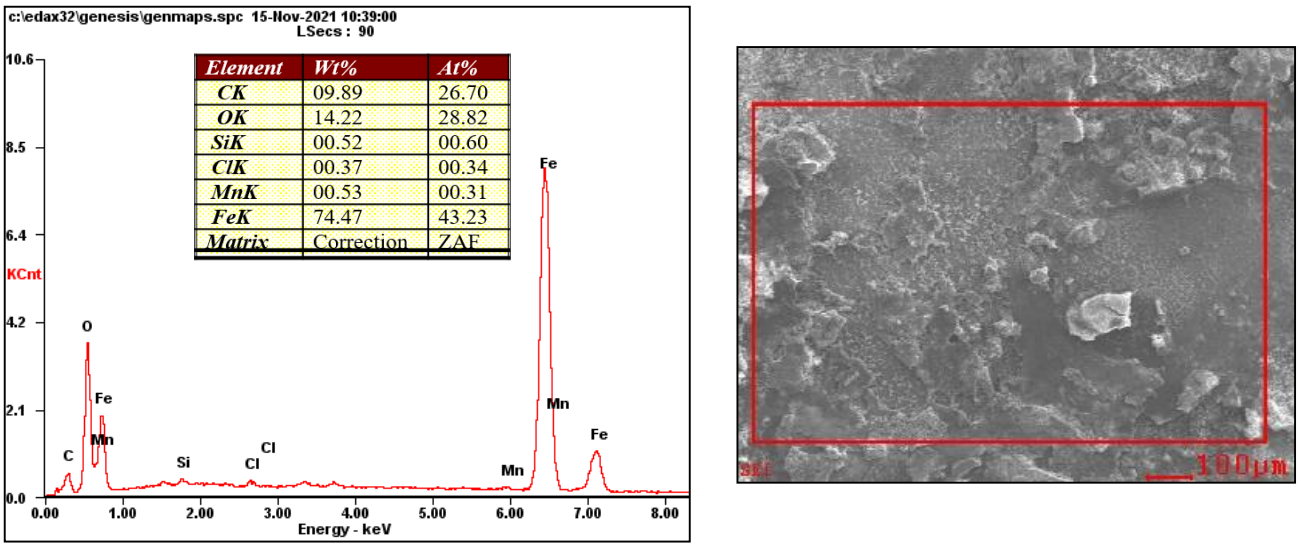


**Figure 12.** EDS of selective corrosion products on X80 steel in sandy soil under the natural air-dried state

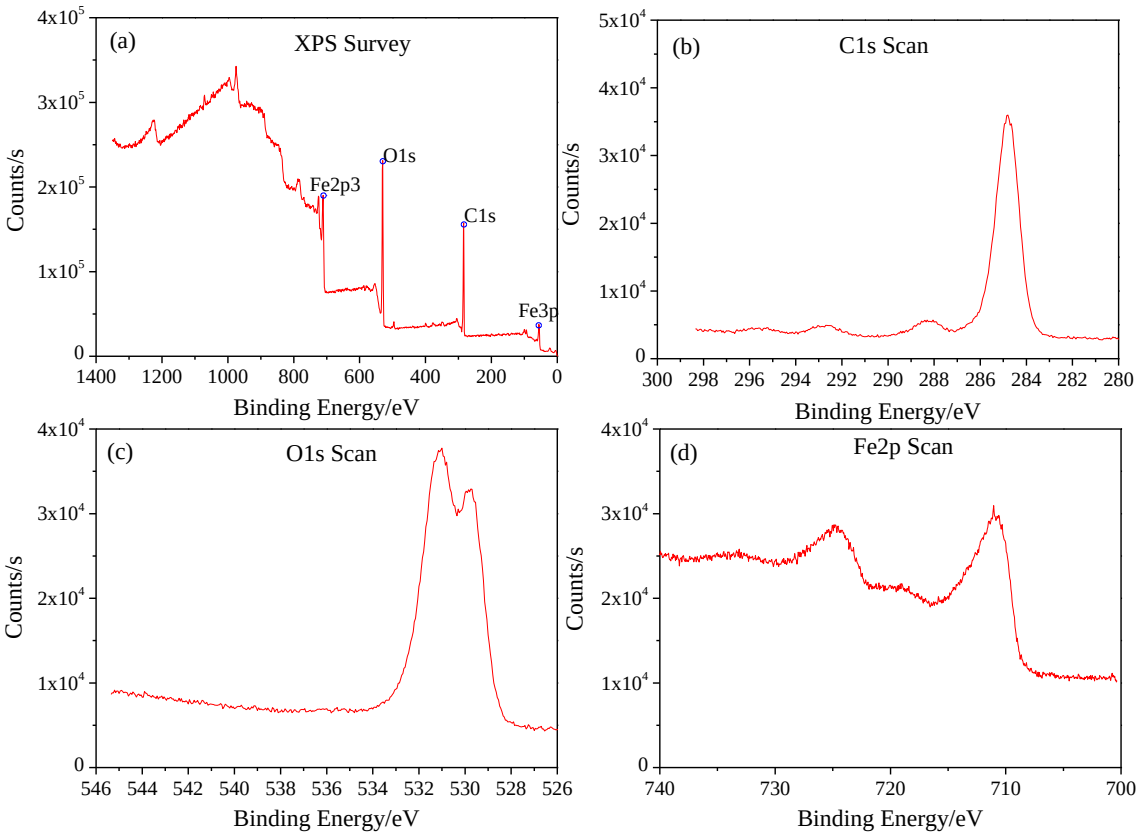


**Figure 13.** XPS of corrosion products on X80 steel in sandy soil under the natural air-dried state

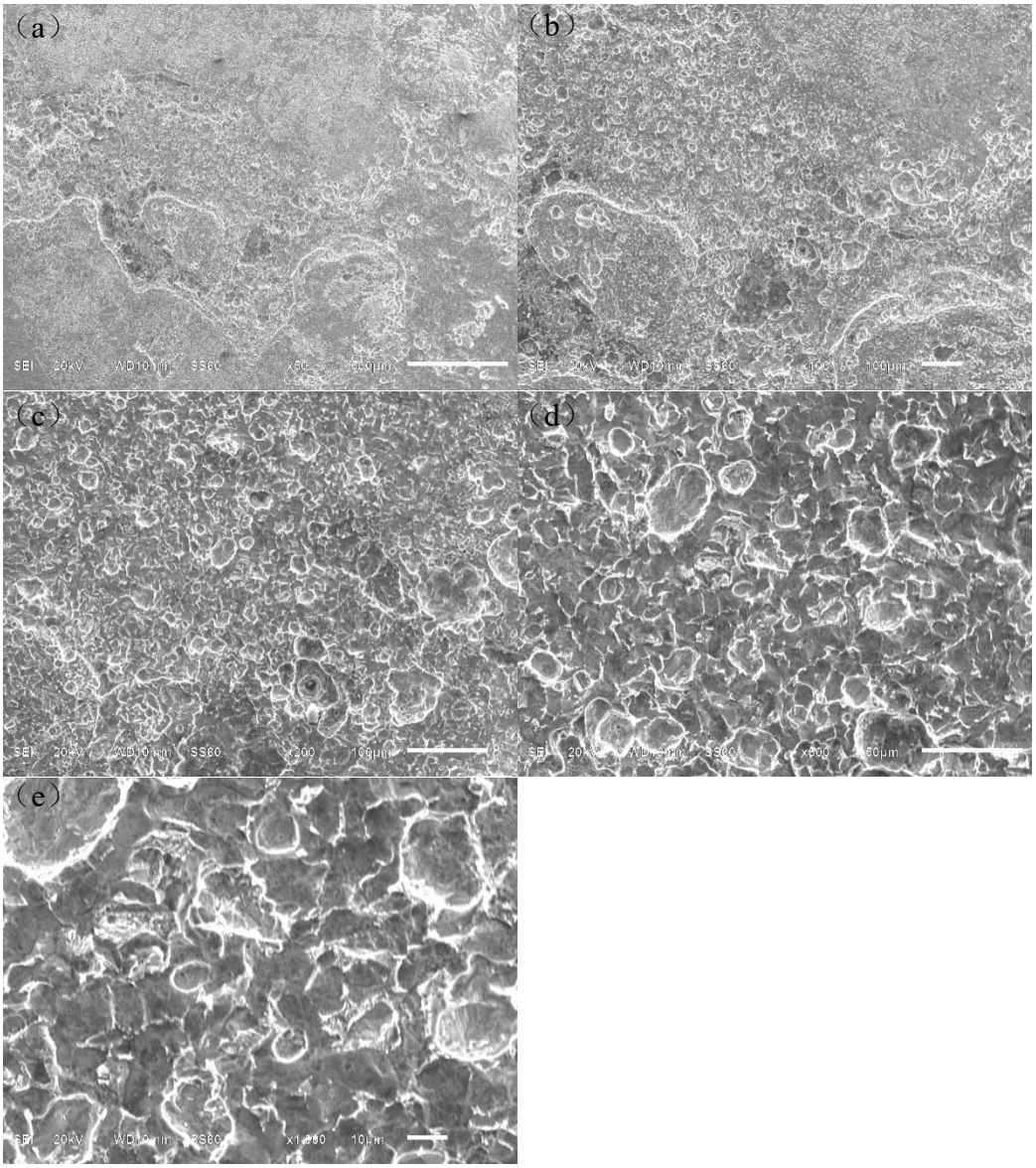


**Figure 14.** Polarization Microscopic corrosion morphology of X80 steel after derusting: (a)×50, (b)×100, (c)×200, (d)×500, (e)×1000

Figure 13 shows the XPS results of corrosion products on the surface of X80 steel. Figure 12(a) shows a full-spectrum scan. The elements of the corrosion products were mainly Fe, O, and C. C may originate from the sample matrix, and Fe and O may originate from the corrosion products. In the fine spectrum of Fe2p (Figure. 13(d)), the characteristic peak located at 710.69 eV represents the formation of oxide $Fe_2O_3$ [23], and the other peaks belong to the corresponding satellite peaks [24]. The products on the surface of X80 steel were mainly $Fe_2O_3$. The $Fe^{2+}$ produced in the anode process may react with $H_2O$ in the neutral pore liquid to form $Fe(OH)_2$ (Equation 3), which is further oxidized to $Fe_2O_3$ deposited on the surface of X80 steel [25].

$$\mathrm{Fe} - 2\mathrm{e} \rightarrow Fe^{2+} \quad (1)$$

$$O_2 + 4H^+ + 4\mathrm{e} \rightarrow 2H_2O \quad (2)$$

$$\mathrm{Fe}^{2+} + 2H_2O \rightarrow \mathrm{Fe}(OH)_2 + 2H^+ \quad (3)$$

$$4\mathrm{Fe}(OH)_2 + O_2 \rightarrow 2\mathrm{Fe}_2O_3 + 4H_2O \quad (4)$$

To further study the corrosion mechanism, SEM morphology analysis was carried out after the corrosion products were removed, and the magnifications were ×50, ×100, ×200, ×500 and ×1000, as shown in Figure 14. The surface corrosion of X80 steel was localized, which was strong in local areas and formed many corrosion pits, while the corrosion of the remaining parts was weak.

## 4. CONCLUSION

Based on the relationships among electrochemical theory, corrosion of sandy soil and corrosion principle of X80 steel, the corrosion mechanism of X80 steel in sand under a natural air-drying state was comprehensively studied in this paper. The following conclusions are drawn:

(1) The pH value of sandy soil fluctuated in a range of 6.85-7.05, the sandy soil was basically neutral, and the temperature fluctuated around 20 °C. The moisture in the sandy soil was gradually air-dried from the initial saturated state of 30% to 0% in 14 days.

(2) As the age increased, as the water content in sandy soil decreased, the polarization curve of the X80 steel shifted to the upper left, and the corrosion effect of the sandy soil to the X80 steel gradually weakened. The corrosion current density $I_o$ were all below 3 μA/cm$^2$, the X80 steel exhibited slight corrosion, and the average corrosion rate was 1.65E-2 mm/a.

(3) In the frequency domain of $10^{-2}$-$10^3$ Hz, the impedance spectrum showed a flat capacitive reactance arc, and the radius of the capacitive reactance arc increased first and then decreased. Near the limit volume content of the liquid bridge, the radius of the capacitive arc was the smallest, and the sandy soil had the strongest corrosion impact on X80 steel.

(4) Brown-yellow corrosion products (iron oxides, $Fe_2O_3$) with uneven thickness were deposited on the surface of the X80 steel. The localized corrosion products appeared as leopard patterns, flocculent clusters, and rice grains, which were strong in local areas and formed many corrosion pits.

ACKNOWLEDGMENTS
The authors would like to express their gratitude to the funding provided by PhD research launch project of Jinzhong University (No. jzxybsjjxm2019019), Scientific and technological innovation projects of colleges and universities in Shanxi Province (No. 2020L0588), Applied Basic Research Program of Shanxi Province (No. 202103021224306), Opening Project of Sichuan University of Science and Engineering, Material Corrosion and Protection Key Laboratory of Sichuan province (No. 2020CL13), National Natural Science Foundation of China (No. 51208333, No. 41807256).

## References

1. C.N. Cao, Natural environmental corrosion of Chinese materials, Chemical Industry Press, (2005) Beijing.
2. Y.P. Hu, *Energy Conserv. Environ. Prot*., 5 (2015) 1.
3. L.X. Zhang, N.M. Lin, J.J. Zou, X.Z. Lin, Z.Q. Liu, S. Yuan, Y. Yu, Z.X. Wang, Q.F. Zeng, W.G. Chen, L.H. Tian, L. Qin, R.Z. Xie, B.Q. Li, Z.H. Wang, B. Tang and Y.C. Wu, *Opt. Laser Technol*., 127 (2020) 106146.
4. X.D. Li, X.J. Li, J. Yang, Z.J. Zhou and C. Ma, *Electr. Power Technol. Environ. Prot*., 30 (2014) 8.

5. J.Q. Zhang, Electrochemical Measurement Technology, Chemical Industry Press, (2010) Beijing.
6. M.L. Shi, AC Impedance Spectroscopy Principles and Applications, National Defence Industry Press, (2001) BeiJing.
7. M.L. Shi, Impedance Spectroscopy of Concrete, China Railway Publishing House, (2003) BeiJing.
8. S.W. Niu, P.G. Han, F.N. Sun, R.Z. Xie, B. He, F.L. Ma, X.G. Guo and A.A. Fattah, *Int. J. Electrochem. Sci.,* 15 (2020) 9428.
9. W.W. Wang, J. Wang and Y.H. Lu, *Corros. Sci. Prot. Technol*. , 21 (2009) 393.
10. B. He, C.H. Lu, P.J. Han and X.H. Bai, *Eng. Fail. Anal., 59* (2016) 410.
11. Y.F. Zhang, P.J. Han and B. He, *J. Taiyuan Univ. Technol*., 48 (2017) 55.
12. Y.H. Wu, S.X. Luo and Q.S. Mou, *Int. J. Electrochem. Sci*., 15 (2020) 576.
13. J. Xu, Y.L. Bai, T.Q. Wu, M.C. Yan, C.K. Yu and C. Sun, *Eng. Fail. Anal*., 100 (2019) 192.
14. F.L. Mi, R.Z. Xie and P.J. Han, *Sci. Technol. Eng*., 18 (2018) 148.
15. R.Z. Qin, H.X. Du, M.X. Lu, L. Ou and H.M. Sun, *Acta Metall. Sin*., 54 (2018) 886.
16. Y. Wu, S.X. Zha and P. W. Jin, *J. Pressure Vessel Technol*., 141 (2019) 1.
17. X.L. Bai, B. He, P.J. Han, R.Z. Xie, F.N. Sun, Z.W. Chen, Y. T. Wang and X.Y. Liu, *RSC Adv*., 12 (2021) 129.
18. X.L. Bai, B. He, P.J. Han, R.Z. Xie, F.N. Sun, Z.W.Chen, X.Y. Liu and Y.T. Wang, *J. Mater. Eng. Perform*., 31 (2021) 476.
19. H.P. Yao, M.C. Yan, X. Yang and C. Sun, *J. Chin. Soc. Corros. Prot*., 34 (2014) 472.
20. H.Y. Tang, G.L. Song, C.N. Cao and H.C. Lin, *Corros. Sci. Prot. Technol*., 8 (1996) 179.
21. R.Z. Xie, P.J. Han, X.Y. Wang, B.Q. Li, B. He, F.L. Ma and X.H. Bai, *Int. J. Electrochem. Sci.,* (2020) 3543.
22. J. Jiang and J. Wang, *Corros. Sci. Prot. Technol*., 21 (2009) 79.
23. H.W. Liu, T.Y. Gu, G.A. Zhang, H.F. Liu and Y. Frank Chen, *Corros. Sci*., 136 (2018) 47.
24. X. Wei, S.C. Zhang, Z. J. Du, P.H. Yang, J. Wang and Y.B. Ren, *Electrochim. Acta*, 107 (2013) 549.
25. Q.L. Zhang, R. Yao, C.X. Yin, P.F. Huang and J. Zhou, *Mater. Prot*., 49 (2016) 62.